

Predominance of the Kitaev interaction in a three-dimensional honeycomb iridate: from *ab-initio* to spin model

Heung-Sik Kim,¹ Eric Kin-Ho Lee,¹ and Yong Baek Kim^{1,2}

¹*Department of Physics and Center for Quantum Materials, University of Toronto, 60 St. George St., Toronto, Ontario, M5S 1A7, Canada*

²*Canadian Institute for Advanced Research / Quantum Materials Program, Toronto, Ontario MSG 1Z8, Canada*

The recently discovered three-dimensional hyperhoneycomb iridate, β -Li₂IrO₃, has raised hopes for the realization of dominant Kitaev interaction between spin-orbit entangled local moments due to its near-ideal lattice structure. If true, this material may lie close to the sought-after quantum spin liquid phase in three dimensions. Utilizing *ab-initio* electronic structure calculations, we first show that the spin-orbit entangled basis, $j_{\text{eff}} = 1/2$, correctly captures the low energy electronic structure. The effective spin model derived in the strong coupling limit supplemented by the *ab-initio* results is shown to be dominated by the Kitaev interaction. We demonstrated that the possible range of parameters is consistent with a non-coplanar spiral magnetic order found in a recent experiment. All of these analyses suggest that β -Li₂IrO₃ may be the closest among known materials to the Kitaev spin liquid regime.

Introduction – Kitaev’s exact solution of a quantum spin-liquid on a spin-1/2 honeycomb model has spurred considerable interest in the search for a material realization[1, 2]. Of particular focus is the family of quasi-two-dimensional (2D) honeycomb iridate materials α -A₂IrO₃ ($A = \text{Na, Li}$, hereafter α AIO), where iridium (Ir) ions form decoupled layers of honeycomb lattices[3, 4] and have been argued to host spin-orbital entangled $j_{\text{eff}} = 1/2$ degrees of freedom[5–7]. Due to the interplay of strong atomic spin-orbit coupling (SOC) and correlation effects, these $j_{\text{eff}} = 1/2$ moments in the ideal α AIO structure interact in the highly anisotropic manner described by the Kitaev model[8]. In addition to these Kitaev-type exchanges, the symmetries of the ideal structure also permit additional exchanges that generate a plethora of interesting phases of matter[9]. In reality, however, these materials possess sizeable monoclinic distortions that deform the octahedral oxygen cages surrounding Ir ions[4, 10]. These distortions lower the symmetry of the system and therefore complicate the description of these materials. Thus far, a consensus on the minimal model required to describe this family of 2D honeycomb iridates has yet been reached; a distortion-free analog of these honeycomb iridates may offer a more direct path towards the realization of Kitaev physics.

The timely discovery and synthesis[11, 12] of the hyperhoneycomb β -Li₂IrO₃ (hereafter β LIO) may present such an exciting opportunity. Much like its 2D counterpart, the Kitaev model on the ideal, 3D hyperhoneycomb lattice supports an exact spin liquid ground state[13–16]. In addition, the distortion-free, classical pseudospin-1/2 model on the hyperhoneycomb lattice also supports a myriad of complex magnetic phases[17]. Moreover, interesting topological phases have been predicted on this lattice[18]. These previous results illustrate the possibilities that may be realizable in β LIO; however, they rely on the use of the $j_{\text{eff}} = 1/2$ degrees of freedom in the low-energy description of β LIO, which has not been justified microscopically. Furthermore, whether the near-ideal structure of β LIO can give rise to a simple minimal pseudospin model dominated by the Kitaev exchange has so far not been validated. Also, with the recent experimental

observation of a magnetic spiral order in β LIO, any minimal model and its accompanying parameters must also be capable of predicting the observed order: this provides a stringent test of feasibility for any model describing β LIO.

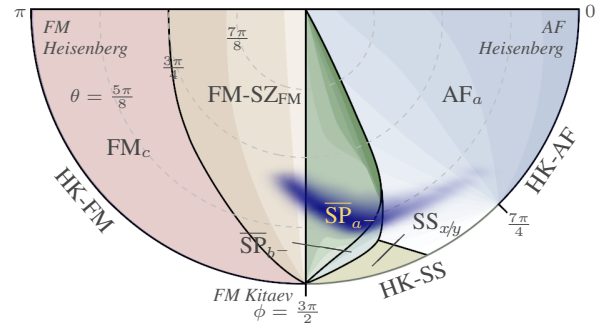


FIG. 1. (Color online) Phase diagram of the J - K - Γ model reproduced from Ref. [17], overlaid with the joint probability density of the exchange interactions estimated from *ab-initio* results for β LIO; see main text for details. The intensity of the blue overlay indicates the likelihood of β LIO belonging in that region of parameter space: the darker a region is, the more probable it is. The most probable region lies close to the ferromagnetic Kitaev region, with small J and Γ as perturbation. The green $\overline{\text{SP}}_{a-}$ spiral phase constitutes a large part of this region. This phase is consistent with the magnetic order observed in the experimental work of Ref. [11]. For detailed discussion of the other phases, see Ref. [17].

In this letter, we tackle these issues by combining results of our *ab-initio* electronic structure calculations and a strong-coupling theory to arrive at a $j_{\text{eff}} = 1/2$ model to describe β LIO. From our *ab-initio* band structure results, we find that the low-energy states can be described in terms of localized $j_{\text{eff}} = 1/2$ states because of the large atomic SOC present in Ir. In fact, the magnitude of SOC in the paramagnetic state is enhanced by the electron interactions in Ir d orbitals, which is consistent with recent observations in several $4d$ and $5d$ transition metal compounds[19–21]. To go beyond the limitation of *ab-initio* calculations in treating electron interactions, we employ the strong-coupling expansion recently proposed in [9] to

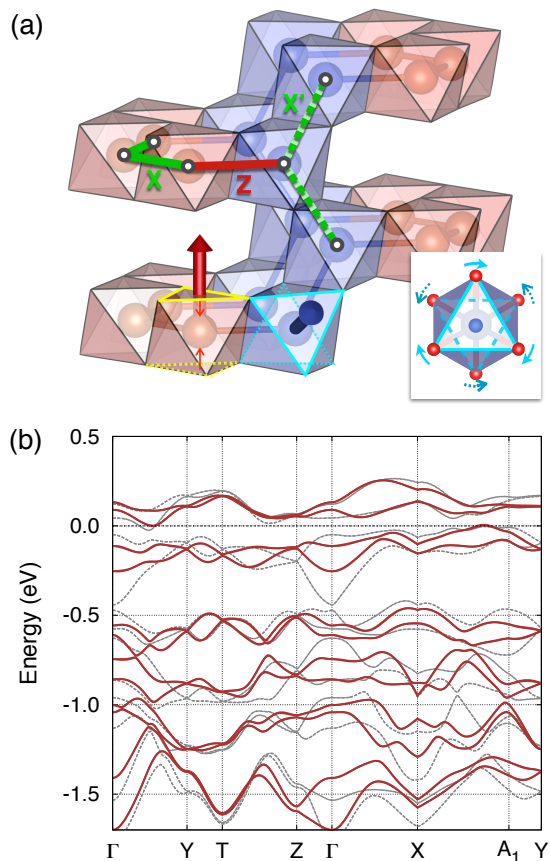


FIG. 2. (Color online) (a) Network of IrO_6 octahedra in the hyperhoneycomb lattice. The two distinct nearest-neighbor (NN) bonds, X and Z, are depicted as solid green and red lines, respectively. X and X' bonds are symmetry equivalent, whereas Z bonds are distinct. Emerging from the octahedra, the red and blue arrows point in the direction of the trigonal distortions for red and blue IrO_6 octahedra respectively. The trigonal distortion, which consists of the compression and rotations of the opposing oxygen triangles, is illustrated in the figure and in the inset. (b) shows the band structure with the presence of spin-orbit coupling (SOC). Solid red and dashed grey curves are the band structure of the experimental and ideal structures, respectively.

arrive at a minimal pseudospin-1/2 model. Due to the near-ideal structure of βLIO , we discover that the resulting pseudospin model is near-isotropic while both distortion-induced and further neighbor interactions are small. Remarkably, the estimated exchange interactions places the model near the ferromagnetic Kitaev limit and within a region where the classical ground state agrees well with the experimentally-observed spiral phase[11]. Our results are summarized in Fig. 1 and elaborated in the rest of this work.

Structure and ab-initio calculations – βLIO is a member of the generic three-dimensional (3D) harmonic honeycomb iridate series[22], which are structural variants of 2D-honeycomb iridates αAIO . The hyperhoneycomb lattice is composed of a tri-coordinated network of edge-shared IrO_6 octahedra as shown in Fig. 2(a). There are two types of

nearest-neighbor (NN) bonds in this network: we denote these bonds as X and Z. Despite being symmetry-inequivalent, these two bonds are almost identical owing to their similar local crystal structures as revealed by recent structural analysis[11, 12].

The crystal structure refinement also revealed nearly ideal IrO_6 octahedra compared to those from αLIO : standard deviations of the Ir-O bond length and O-Ir-O bond angles in βLIO (0.002 Å and 2.77°) are much smaller than those in αLIO (0.050 Å and 4.56°)[10]. Since finite standard deviations in O-Ir-O bond angles is a result of trigonal distortion in the IrO_6 octahedra, the small value present in βLIO indicates that trigonal distortions are indeed small in this compound (the directions of trigonal distortion are shown as colored arrows in the figure). The nearly ideal IrO_6 octahedra in βLIO suggest that local crystal fields are principally cubic in symmetry, therefore the spin-orbital entangled $j_{\text{eff}} = 1/2$ states would be a good basis to construct a low-energy description of this material in the presence of strong SOC.

To validate the use of $j_{\text{eff}} = 1/2$ states in the low-energy description of βLIO , we turn to *ab-initio* electronic structure calculations (see Supplementary Materials for details). The band dispersions of the ideal and experimental structures with SOC can be seen in Fig. 2(b). The dispersions from the experimental structure (solid red curves) and those from ideal one (dashed grey curves) share similar overall shape, especially near the chemical potential. The separation between the upper eight bands and the lower sixteen bands (including Kramers degeneracies) can be clearly seen in the figure, suggesting the formation of $j_{\text{eff}} = 1/2$ and $j_{\text{eff}} = 3/2$ bands[23].

In Fig. 3(a), we show the $j_{\text{eff}} = 1/2$ -projected band dispersions and density of state (PDOS) in the presence of SOC based on the experimental structure. The large $j_{\text{eff}} = 1/2$ PDOS weight in the upper eight bands—the closest bands to the Fermi level—indicates the development of $j_{\text{eff}} = 1/2$ bands and confirms that the basis states relevant to the low-energy description of βLIO possess mostly $j_{\text{eff}} = 1/2$ character. The effect of electron correlations inherent to Ir t_{2g} orbital further enhances the $j_{\text{eff}} = 1/2$ character as shown in Fig. 3(b), where effective on-site Coulomb interaction $U_{\text{eff}} \equiv U - J_H$ is included within the DFT+ U formalism (J_H is Hund's coupling; for details see Supplementary Materials).[24] As $U_{\text{eff}} = 3.0$ eV is added, the separation between the $j_{\text{eff}} = 1/2$ and $j_{\text{eff}} = 3/2$ states becomes enlarged. This SOC enhancement is also manifested in the increase of SOC magnitudes $\lambda_{t_{2g}}$ in the t_{2g} states as shown in Table I. Such behavior has also been reported in other 4d and 5d orbital systems [25][19–21].

The effects caused by electron correlations in the low-energy $j_{\text{eff}} = 1/2$ -dominated states deserve further comment. Fig. 3(c) shows the schematic shape of Wannier orbitals constructed from the $j_{\text{eff}} = 1/2$ energy window, which can be considered as the local orbitals that span the low-energy subspace. Owing to the nearly ideal IrO_6 octahedra (as supported by the small amount of trigonal distortion of less than 100 meV), the Wannier orbitals consist of pure $j_{\text{eff}} = 1/2$

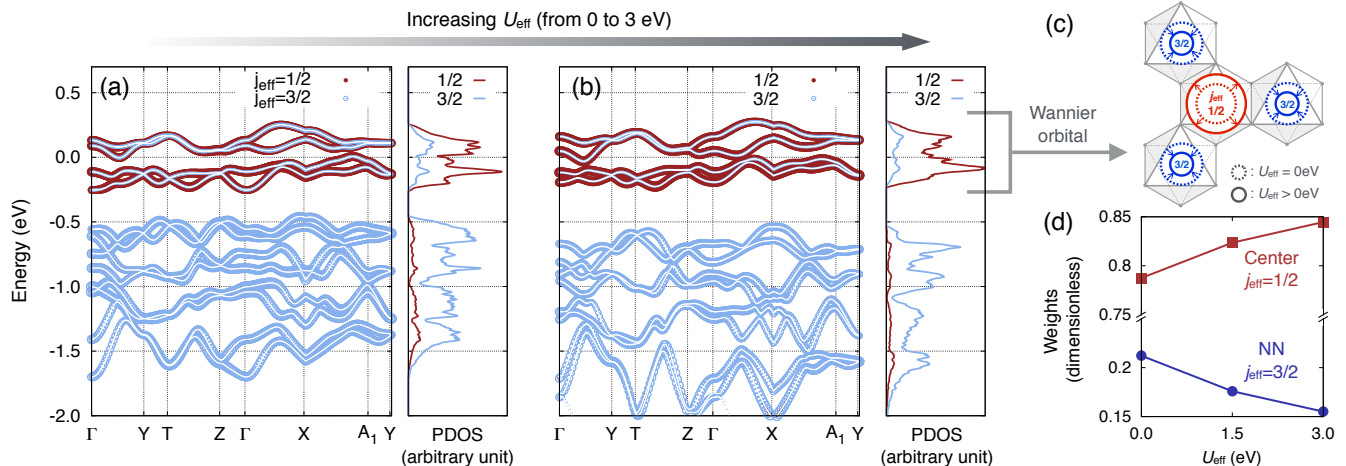


FIG. 3. (Color online) (a,b) Band structure and density of states (DOS) projected onto the j_{eff} states in the presence of SOC (a) without and (b) with the on-site Coulomb interaction $U_{\text{eff}} = 3.0$ eV. (c) shows the schematic shape of the $j_{\text{eff}}=1/2$ -like Wannier orbital constructed from the $j_{\text{eff}}=1/2$ -dominated bands near the Fermi level. Dashed and solid circles depict the Wannier orbitals from calculations without and with finite U_{eff} , respectively. Weights of the central $j_{\text{eff}}=1/2$ and nearest-neighboring $j_{\text{eff}}=3/2$ tail in the orbital are shown in (d) as a function of U_{eff} .

U_{eff} (eV)	0.0	1.5	3.0
$\lambda_{t_{2g}}$	0.401	0.482	0.516
t_1			
Z	+0.085	+0.077	+0.064
X	+0.083	+0.074	+0.058
$ t_2 $			
Z	0.238	0.255	0.270
X	0.260	0.276	0.289
t_3			
Z	-0.162	-0.119	-0.060
X	-0.153	-0.110	-0.055

TABLE I. Magnitude of SOC within the Ir t_{2g} states and t_{2g} hopping terms from Wannier orbital calculations in the presence of U_{eff} . We adopt the coordinate system such that t_2 is negative for both Z and X bonds. By symmetry, t_2 is positive for the X' bonds.

character on the center Ir site, while it has $j_{\text{eff}} = 3/2$ tails on the NN sites. Similar features have been reported in α NIO and α LIO[26, 27], which mirrors the remnant molecular orbital character originating from the t_{2g} hopping[28]. As U_{eff} is included and $\lambda_{t_{2g}}$ is enhanced, the $j_{\text{eff}} = 1/2$ character becomes more dominant while $j_{\text{eff}} = 3/2$ components on the NN sites decreases as shown in Fig. 3(c) and (d). The $j_{\text{eff}} = 1/2$ -like Wannier orbital is more localized accordingly, which makes the low-energy description of β LIO in terms of the localized $j_{\text{eff}} = 1/2$ states more feasible in the strong coupling limit.

t_{2g} Wannier orbital hopping amplitudes – For a detailed understanding of how the near-ideal structure of β LIO is manifested in the electronic band structure, we calculated the Ir t_{2g} hopping amplitudes from the Wannier orbitals in the experimental structure. Table I shows the magnitude of the three largest hopping terms— t_1 , t_2 , and t_3 —as the value of U_{eff} changes ($U_{\text{eff}} = 0.0$ eV, 1.5 eV, and 3.0 eV, and SOC is included in the calculation); see Fig. S1(a) in Supplementary Materials and Ref. [29] for illustration of these hopping processes. Since the Ir-Ir bond lengths and Ir-O-Ir bond angles are similar on the two inequivalent bonds of β LIO (X and

Z bonds), the values of their respective hopping amplitudes are expected to be similar. Indeed, by comparing the hopping amplitudes between the two inequivalent NN bonds, we observe small anisotropies between the X and Z bonds ($< 10\%$), which reflects the close-to-ideal structure of β LIO.

The evolution of the NN hopping amplitudes as we include on-site Coulomb interactions can be seen in Table I. As U_{eff} increases, $|t_2|$ increases while t_1 and t_3 decrease. Such behavior is understood in terms of the enhanced hybridization between the Ir t_{2g} and oxygen p states in the presence of U_{eff} . Inclusion of U_{eff} pushes the $j_{\text{eff}}=3/2$ states down energetically so that they become closer to the oxygen p states. This leads to increased hybridization between the Ir t_{2g} and oxygen p states, which yields the enhancement of oxygen-mediated t_2 (and the reduction of t_1 and t_3).

Strong-coupling minimal model and experimental spiral phase – Having validated the use of the $j_{\text{eff}} = 1/2$ basis and the similarity of hopping amplitudes between inequivalent bonds, we can now construct an effective model to describe the low-energy properties of β LIO in the large- U limit. Following the derivation in Ref. [9], we start with localized $j_{\text{eff}} = 1/2$ states then perform a strong-coupling expansion using NN t_{2g} hopping amplitudes. In the presence of Hund's coupling J_H , we arrive at a NN, $j_{\text{eff}} = 1/2$ model with highly anisotropic pseudospin exchanges

$$H = \sum_{\langle ij \rangle \in \alpha(\beta\gamma)} J^\alpha S_i \cdot S_j + K^\alpha S_i^\alpha S_j^\alpha + \Gamma^\alpha (S_i^\beta S_j^\gamma + S_i^\gamma S_j^\beta),$$

where S_i is the $j_{\text{eff}} = 1/2$ pseudospin on site i , α labels the NN $\langle ij \rangle$ bond by its Kitaev component, and β and γ denote the two non-Kitaev components of the $\langle ij \rangle$ -bond. The exchanges J , K , and Γ are functions of the hopping amplitudes t_1 - t_3 , strength of Hund's coupling J_H , SOC λ , and the on-site Coulomb interaction U : the relation between these quantities are given in Supplementary Materials.

To establish the region in exchange parameter space that best models β LIO, we employ the following statistical analysis. First, we interpolated the hopping amplitudes and SOC values in Table I as a function of U_{eff} . Then, treating both U_{eff} and J_H as independent random variables with ranges 1-3 eV and 50-300 meV respectively[30], we determined the resulting joint probability density of the exchange parameters. From this, we find that the mean anisotropies between X and Z bonds in J , K , and Γ are 3%, 15%, and $< 1\%$ respectively relative to the largest energy scale, which is the Kitaev exchange. As a first approximation, we treat all exchanges as isotropic between the X and Z bonds, which yields the NN Hamiltonian studied in the classical limit in Ref. [17]. Lastly, we overlay the joint probability density function of the exchange parameters on top of the relevant portion of the classical phase diagram reproduced from Ref. [17], thereby yielding Fig. 1. The intensity of the overlay illustrates the probability density: the darker the overlay in a region is, the higher its probability density. We interpret this probability density as the likelihood that the real material belongs in that region of parameter space.

The phase diagram is the bottom half of a polar plot: The angular coordinate ϕ shows the ratio between J and K — $\tan(\phi) = J/K$. Meanwhile, the radial coordinate depicts the strength of Γ — $r \in (0, \pi/2)$, $\tan(\pi - r) = \sqrt{J^2 + K^2}/\Gamma$. The bottom boundary of the half-ring is the Heisenberg-Kitaev limit ($\Gamma = 0$) and the origin is the pure Γ limit. As seen in the figure, the NN exchanges in β LIO are likely dominated by a large, ferromagnetic Kitaev exchange, perturbed by small $|J|$ and $|\Gamma|$.

We find the spiral phase $\overline{\text{SP}}_{a^-}$ in green comprises a large fraction of the region of highest probability density. Remarkably, this non-coplanar spiral magnetic phase possesses the same symmetries as the experimentally determined magnetic order.[11, 17] In other words, using the *ab-initio* hopping and SOC parameters, the resulting exchange parameters in the isotropic J - K - Γ pseudospin model results in a classical ground state that agrees with the experimental magnetic order.

Discussion and Conclusion – Although we have shown that the $j_{\text{eff}} = 1/2$ states form a valid basis as a consequence of the small amount of distortions present, the difference between the dispersions of the ideal and experimental structures away from the Fermi level are due to these distortions and the resulting bond anisotropies. However, in the context of the effective pseudospin model, we have shown that these non-idealities are negligible for the J and Γ exchanges. The Kitaev exchange, on the other hand, is more anisotropic between the X and Z bonds, but we speculate that the $\overline{\text{SP}}_{a^-}$ spiral phase will remain robust under this anisotropy; we leave the investigation on the effects of bond anisotropy for future work. Nevertheless, it remains true that the NN exchanges on both X and Z bonds are dominated by large ferromagnetic Kitaev exchanges and that the Kitaev spin liquid is robust against bond-anisotropies.[1]

In addition to distortions and bond anisotropies, an accurate

description of the electronic structure also requires hopping amplitudes beyond the NN level (see Supplementary Materials for details). Although these terms would generate further neighbor exchange interactions in the strong coupling theory, these exchanges are no more than 10% of those at the NN level. In this regard, we focused on the NN exchange interactions in the analysis of the pseudospin model.

To enhance the Kitaev exchange relative to other interactions and to approach the spin-liquid regime of the Kitaev model, strengthening the oxygen-mediated-type hopping (t_2) is a viable option. Increasing the on-site Coulomb interaction can further localize the t_{2g} orbitals, which reduces the amplitudes for direct hopping channels like t_1 and t_3 while oxygen-mediated hopping channels like t_2 are comparatively less affected. In addition, increasing U has the effect of driving the system deeper into the Mott insulating regime and reducing the strength of further neighbor interactions. Therefore, a $4d$ variant of the β LIO may offer the right ingredients to enhance the Kitaev exchange.

Indeed, the isoelectronic, 2D honeycomb α -Li₂RhO₃ has been synthesized and argued to be a relativistic Mott insulator driven by electronic correlations and SOC.[31] Furthermore, this material does not magnetically order down to 0.5 K, which is an indication of magnetic frustration.[31] We speculate that the hypothetical 3D polymorph—hyperhoneycomb β -Li₂RhO₃—may be a less distorted version of α -Li₂RhO₃ that has all the right properties to further approach the Kitaev region, in analogy to β LIO.

Acknowledgement – This work was supported by the NSERC of Canada and the center for Quantum Materials at the University of Toronto. Computations were mainly performed on the GPC supercomputer at the SciNet HPC Consortium. SciNet is funded by: the Canada Foundation for Innovation under the auspices of Compute Canada; the Government of Ontario; Ontario Research Fund - Research Excellence; and the University of Toronto. HSK thanks to IBS Center for Correlated Electron System in Seoul National University for additional computational resources.

-
- [1] A. Kitaev, *Ann. Phys.* **321**, 2 (2006).
 - [2] Y. Singh, S. Manni, J. Reuther, T. Berlijn, R. Thomale, W. Ku, S. Trebst, and P. Gegenwart, *Phys. Rev. Lett.* **108**, 127203 (2012).
 - [3] S. K. Choi, R. Coldea, A. N. Kolmogorov, T. Lancaster, I. I. Mazin, S. J. Blundell, P. G. Radaelli, Y. Singh, P. Gegenwart, K. R. Choi, S.-W. Cheong, P. J. Baker, C. Stock, and J. Taylor, *Phys. Rev. Lett.* **108**, 127204 (2012).
 - [4] F. Ye, S. Chi, H. Cao, B. C. Chakoumakos, J. A. Fernandez-Baca, R. Custelcean, T. F. Qi, O. B. Korneta, and G. Cao, *Phys. Rev. B* **85**, 180403(R) (2012).
 - [5] B. Kim, H. Jin, S. Moon, J.-Y. Kim, B.-G. Park, C. Leem, J. Yu, T. Noh, C. Kim, S.-J. Oh, *et al.*, *Phys. Rev. Lett.* **101**, 076402 (2008).
 - [6] A. Shitade, H. Katsura, J. Kuneš, X.-L. Qi, S.-C. Zhang, and N. Nagaosa, *Phys. Rev. Lett.* **102**, 256403 (2009).

- [7] H. Gretarsson, J. P. Clancy, X. Liu, J. P. Hill, E. Bozin, Y. Singh, S. Manni, P. Gegenwart, J. Kim, A. H. Said, D. Casa, T. Gog, M. H. Upton, H.-S. Kim, J. Yu, V. M. Katukuri, L. Hozoi, J. Van Den Brink, and Y.-J. Kim, *Phys. Rev. Lett.* **110**, 076402 (2013).
- [8] G. Jackeli and G. Khaliullin, *Phys. Rev. Lett.* **102**, 017205 (2009).
- [9] J. G. Rau, E. K.-H. Lee, and H.-Y. Kee, *Phys. Rev. Lett.* **112**, 077204 (2014).
- [10] M. J. O'Malley, H. Verweij, and P. M. Woodward, *Journal of Solid State Chemistry* **181**, 1803 (2008).
- [11] A. Biffin, R. D. Johnson, S. Choi, F. Freund, S. Manni, A. Bombardi, P. Manuel, P. Gegenwart, and R. Coldea, *Phys. Rev. B* **90**, 205116 (2014).
- [12] T. Takayama, A. Kato, R. Dinnebier, J. Nuss, and H. Takagi, [arXiv:1403.3296](https://arxiv.org/abs/1403.3296) (2014).
- [13] S. Mandal and N. Surendran, *Phys. Rev. B* **79**, 024426 (2009).
- [14] E. K.-H. Lee, R. Schaffer, S. Bhattacharjee, and Y. B. Kim, *Phys. Rev. B* **89**, 045117 (2014).
- [15] I. Kimchi, J. G. Analytis, and A. Vishwanath, [arXiv:1309.1171](https://arxiv.org/abs/1309.1171) (2013).
- [16] J. Nasu, T. Kaji, K. Matsuura, M. Udagawa, and Y. Motome, *Phys. Rev. B* **89**, 115125 (2014).
- [17] E. K.-H. Lee and Y. B. Kim, [arXiv:1407.4125](https://arxiv.org/abs/1407.4125) (2014).
- [18] R. Schaffer, E. K.-H. Lee, Y.-M. Lu, and Y. B. Kim, [arXiv:1409.5125](https://arxiv.org/abs/1409.5125) (2014).
- [19] G.-Q. Liu, V. N. Antonov, O. Jepsen, and O. K. Andersen, *Phys. Rev. Lett.* **101**, 026408 (2008).
- [20] H.-S. Kim, Y. Chen, and H.-Y. Kee, [arXiv:1411.1406](https://arxiv.org/abs/1411.1406) (2014).
- [21] V. V. Shankar, H.-S. Kim, and H.-Y. Kee, [arXiv:1411.6623](https://arxiv.org/abs/1411.6623) (2014).
- [22] K. A. Modic, T. E. Smidt, I. Kimchi, N. P. Breznay, A. Biffin, S. Choi, R. D. Johnson, R. Coldea, P. Watkins-Curry, G. T. McCandless, J. Y. Chan, F. Gandara, Z. Islam, A. Vishwanath, A. Shekhter, R. D. McDonald, and J. G. Analytis, *Nature Comm.* **5**, 4203 (2014).
- [23] We comment that, due to the loss of chiral symmetry and the mixing of the $j_{\text{eff}} = 3/2$ states in the $j_{\text{eff}} = 1/2$ subspace, the nodal Fermi ring mentioned in previous tight-binding analysis is absent in both of the ideal and experimental structures.
- [24] In order to capture the role of electron correlations in the electronic structure only, we do not consider any magnetism in our DFT+ U calculations in this work.
- [25] We note this SOC enhancement in β LIO is less significant compared to other systems because the $j_{\text{eff}} = 1/2$ and $3/2$ states were already well-separated when $U_{\text{eff}} = 0$ eV as a result of large SOC.
- [26] H.-S. Kim, C. H. Kim, H. Jeong, H. Jin, and J. Yu, *Phys. Rev. B* **87**, 165117 (2013).
- [27] C. H. Sohn, H.-S. Kim, T. F. Qi, D. W. Jeong, H. J. Park, H. K. Yoo, H. H. Kim, J.-Y. Kim, T. D. Kang, D.-Y. Cho, G. Cao, J. Yu, S. J. Moon, and T. W. Noh, *Phys. Rev. B* **88**, 085125 (2013).
- [28] I. I. Mazin, H. O. Jeschke, K. Foyevtsova, R. Valentí, and D. I. Khomskii, *Phys. Rev. Lett.* **109**, 197201 (2012).
- [29] C. H. Kim, H. S. Kim, H. Jeong, H. Jin, and J. Yu, *Phys. Rev. Lett.* **108**, 106401 (2012).
- [30] For both U_{eff} and J_H , we chose triangular distributions for the stated range. The qualitative features of the resulting exchange parameters' probability densities are not dependent on the precise distribution used but only on the mean and range of the distribution.
- [31] Y. Luo, C. Cao, B. Si, Y. Li, J. Bao, H. Guo, X. Yang, C. Shen, C. Feng, J. Dai, *et al.*, *Phys. Rev. B* **87**, 161121 (2013).
- [32] T. Ozaki, *Phys. Rev. B* **67**, 155108.
- [33] <http://www.openmx-square.org>.
- [34] J. P. Perdew, K. Burke, and M. Ernzerhof, *Phys. Rev. Lett.* **77**, 3865 (1996).
- [35] D. M. Ceperley and B. J. Alder, *Phys. Rev. Lett.* **45**, 566 (1980).
- [36] J. P. Perdew and A. Zunger, *Phys. Rev. B* **23**, 5048 (1981).
- [37] M. J. Han, T. Ozaki, and J. Yu, *Phys. Rev. B* **73**, 045110 (2006).
- [38] N. Marzari and D. Vanderbilt, *Phys. Rev. B* **56**, 12847 (1997).
- [39] H. Weng, T. Ozaki, and K. Terakura, *Phys. Rev. B* **79**, 235118 (2009).
- [40] E. K.-H. Lee, S. Bhattacharjee, K. Hwang, H.-S. Kim, H. Jin, and Y. B. Kim, *Phys. Rev. B* **89**, 205132 (2014).

Supplementary Material A:
Details on *ab-initio* electronic structure calculations

For the electronic structure calculations with SOC and on-site Coulomb interaction, OPENMX code[32, 33], which is based on the linear-combination-of-pseudo-atomic-orbital basis formalism, was used. A non-collinear DFT scheme and a fully relativistic j -dependent pseudopotential were used to treat SOC, and Perdew-Burke-Ernzerhof parametrization of the generalized gradient approximation (GGA) was chosen for the exchange-correlation functional[34], which was compared and found to be almost identical with the results with the Perdew and Zunger local density approximation functional[35, 36]. 400 Ry of energy cutoff was used for the real-space sampling, and $9 \times 9 \times 9$ k -grid was adopted for the primitive unit cell. Electron interactions are treated as on-site Coulomb interactions via a simplified LDA+ U formalism implemented in OPENMX code[37], and up to 3.0 eV of $U_{\text{eff}} \equiv U - J_{\text{H}}$ parameter (J_{H} is Hund's coupling) was used for Ir d orbital in our GGA+SOC+ U calculations. Maximally-localized Wannier orbital method[38], which is implemented in OPENMX code[39], were used to obtain the tight-binding Hamiltonian for Ir t_{2g} atoms.

Supplementary Material B:
 t_{2g} hopping terms from Wannier orbitals

Table S1 shows a partial list of Ir t_{2g} hopping terms (up to third NN) from the Wannier orbitals, where the convention for the coordinate system and the illustration of NNN and third NN hopping terms are in Fig. S1. Full list of hopping terms can be restored by applying the C_2 rotations and inversion operations at the centers of Z and X (X') bonds, respectively. Three C_2 rotations — $C_2^{a,b,z}$ — are allowed, where $a \equiv \hat{x} + \hat{y}$ and $b \equiv \hat{y} - \hat{x}$.

TABLE S1: A subset of Ir t_{2g} hopping terms \mathbf{T}_{ij} as representatives of each hopping channels up to third NN, where $\mathcal{H}_{\text{hop}} = \sum_{ij} \mathbf{C}_i^\dagger \cdot \mathbf{T}_{ij} \cdot \mathbf{C}_j$ and \mathbf{C}^\dagger and \mathbf{C} being the creation and annihilation operator for t_{2g} states, respectively. d is approximate distance between Ir and O. Other hopping terms can be recovered by applying $\mathbf{T}_{ji} = \mathbf{T}_{ij}^\dagger$, $C_2^{a,b,z}$ rotations, and inversion operations.

Kind	\mathbf{r}_{ij} (in Cartesian coord.)	Sublattice	$U_{\text{eff}} = 0.0$ eV			$U_{\text{eff}} = 1.5$ eV			$U_{\text{eff}} = 3.0$ eV			
			d_{xy}	d_{xz}	d_{yz}	d_{xy}	d_{xz}	d_{yz}	d_{xy}	d_{xz}	d_{yz}	
t_{NN}	X, X' $(-d, 0, +d)$	1 \rightarrow 4	d_{xy}	+0.088	+0.018	+0.260	+0.080	+0.019	+0.276	+0.064	+0.021	+0.289
d_{xz}			+0.018	-0.152	+0.013	+0.020	-0.110	+0.013	+0.021	-0.051	0.005	
d_{yz}			+0.259	+0.013	+0.078	+0.276	+0.013	+0.067	+0.288	0.003	+0.052	
t_{NN}	Z $(+d, +d, 0)$	1 \rightarrow 2	d_{xy}	-0.162	-0.022	+0.021	-0.119	-0.024	+0.023	-0.059	-0.031	+0.030
d_{xz}			+0.016	+0.087	-0.239	+0.017	+0.078	-0.255	+0.025	+0.072	-0.269	
d_{yz}			-0.016	-0.239	+0.086	-0.017	-0.254	+0.077	-0.024	-0.271	+0.056	
$t_{\text{NNN}}^{\text{I}}$			d_{xy}	d_{xz}	d_{yz}	d_{xy}	d_{xz}	d_{yz}	d_{xy}	d_{xz}	d_{yz}	

Continued in next page...

Contrary to the relatively simple NN hopping channels as shown in the inset of Fig. S1(a), a number of distinct NNN hopping terms are introduced due to the three-dimensional twisting of the honeycomb lattice[40]. The NNN hopping channels can be classified into two kinds, depending on whether they are analogous to the NNN hopping in the 2D honeycomb lattice or not. Fig. S1(b) shows the 2D-like NNN hopping channels, which can be reached through one intermediate NN Ir site. Depending on whether they belong to same zigzag chain composed of only X (or X') bonds or connect different chains, they are divided into two different classes $t_{\text{NNN}}^{\text{I}}$ and $t_{\text{NNN}}^{\text{II}}$. Hopping amplitudes in these channels are larger than the other channels, $t_{\text{NNN}}^{\text{III}}$ and $t_{\text{NNN}}^{\text{IV}}$, which cannot be reached through one Ir site as shown in Fig. S1(c). There are also non-negligible third NN hopping terms, $t_{\text{3NN}}^{\text{I}}$ and $t_{\text{3NN}}^{\text{II}}$, which can be seen in Fig. S1(d) and Table S1. Like NNN hopping channels, third NN channels can be classified depending on whether they have their 2D counterparts or not. $t_{\text{3NN}}^{\text{I}}$ resembles the third NN hopping channel in the 2D honeycomb lattice, while $t_{\text{3NN}}^{\text{II}}$ is similar to the interlayer hopping terms in αAlO series.

Supplementary Material C:
NN exchange interactions

The exchanges J , K , and Γ are given by (suppressing the bond label α)

$$J = \frac{4}{27} \left[\frac{(2t_1 + t_3)^2(4J_{\text{H}} + 3U)}{U^2} - \frac{16J_{\text{H}}(t_1 - t_3)^2}{(2U + 3\lambda)^2} \right]$$

$$K = \frac{32J_{\text{H}}}{9} \left[\frac{(t_1 - t_3)^2 - 3t_2^2}{(2U + 3\lambda)^2} \right], \Gamma = \frac{64J_{\text{H}}}{9} \frac{t_2(t_1 - t_3)}{(2U + 3\lambda)^2}, \quad (1)$$

where t_i ($i = 1, 2, 3$), J_{H} , U , and λ are the NN hopping amplitudes, Hund's coupling, on-site Coulomb repulsion, and SOC respectively[9]. t_i is illustrated in Fig. S1(a).

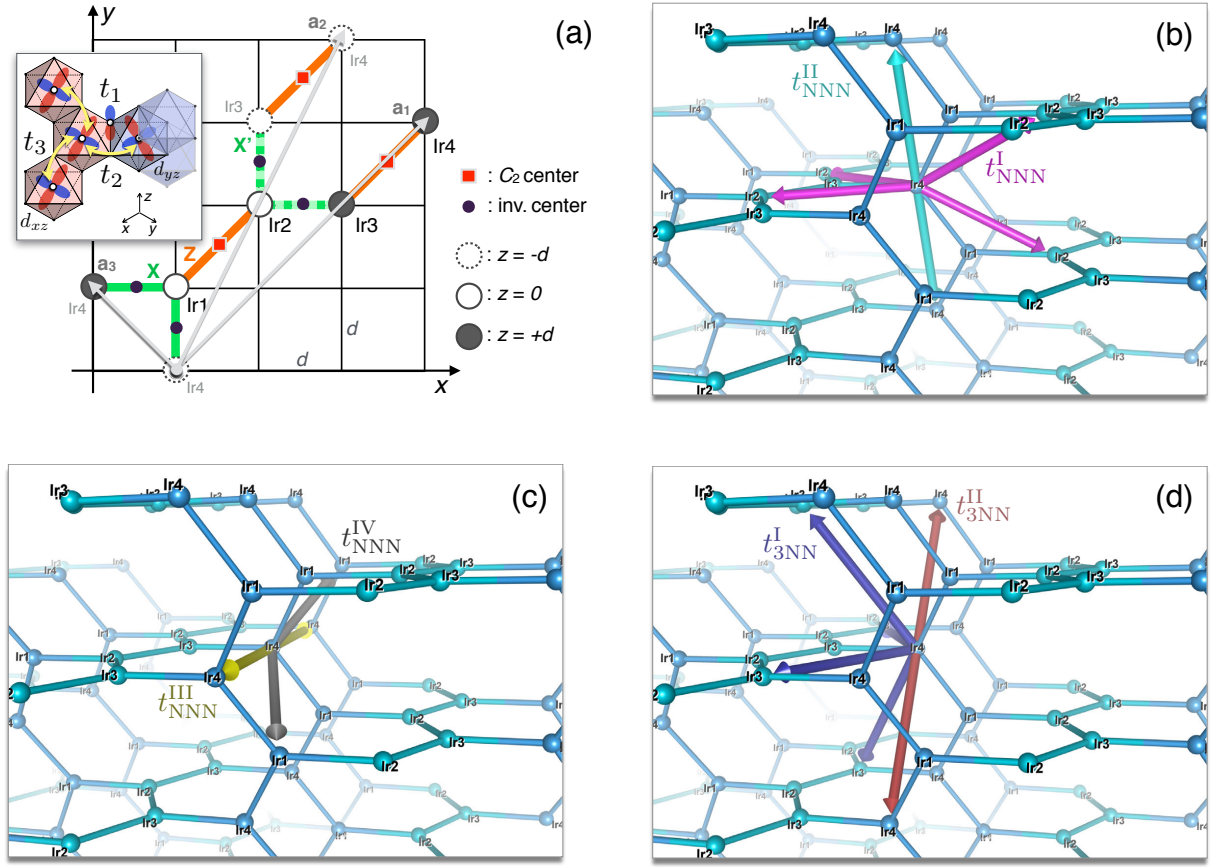


FIG. S1. (Color online) (a) Ir sites projected onto xy -plane defined in terms of local cubic axes. \mathbf{a}_1 , \mathbf{a}_2 and \mathbf{a}_3 are the Bravais lattice vector for the primitive cell, where four sublattices within the primitive cell are labeled as Ir1 to Ir4. Centers for $C_{2v}^{d,b,z}$ rotations and inversion are depicted as red square and black dots on the Z and X (X') bonds, respectively. Note that d becomes same with the Ir-O bond length in the absence of trigonal distortion. Inset shows the three major hopping channels between NN Ir sites. (b,c) All NNN and (d) third NN neighbors for an Ir site, Ir4, are depicted as colored arrows. Note that different colors (blue and green) are used to distinguish Ir sites and bonds belonging to one zigzag chain to another. (a) shows NNN hopping paths that can be reached through intermediate NN Ir sites. Intra- and inter-chain bonds are colored as cyan and purple, respectively. (b) shows NNN paths that cannot be reached through one NN bonds. Yellow and grey arrows represent paths connecting same (Ir4 to Ir4) and different sublattices (Ir4 to Ir1 in the figure), respectively. (c) shows all third NN hopping paths. Purple and red arrows show bonds connecting different and same sublattices, respectively. Note that, bonds in (b) and red bonds in (c) does not have any counterparts in the 2D honeycomb lattice.

Continued from previous page...

Kind	\mathbf{r}_{ij} (in Cartesian coord.)	Sublattice	$U_{\text{eff}} = 0.0 \text{ eV}$			$U_{\text{eff}} = 1.5 \text{ eV}$			$U_{\text{eff}} = 3.0 \text{ eV}$			
	$(+d,+2d,-d)$	$1 \rightarrow 3$	d_{xy}	0.002	-0.012	+0.039	0.001	-0.015	+0.044	0.001	-0.018	+0.047
			d_{xz}	+0.013	0.001	+0.011	+0.018	0.001	+0.014	+0.024	0.001	+0.017
			d_{yz}	+0.063	0.004	0.002	+0.075	0.007	0.000	+0.089	-0.010	0.001
$t_{\text{NNN}}^{\text{II}}$	$(-d,+d,+2d)$	$1 \rightarrow 1$	d_{xy}	0.002	0.008	-0.014	0.003	-0.011	-0.017	0.003	-0.014	-0.020
			d_{xz}	+0.014	0.001	+0.039	+0.017	0.000	+0.045	+0.020	0.002	+0.050
			d_{yz}	0.008	+0.075	0.001	+0.011	+0.089	0.000	+0.014	+0.103	0.001
$t_{\text{NNN}}^{\text{III}}$	$(-d,+d,-2d)$	$1 \rightarrow 1$	d_{xy}	0.001	+0.011	0.001	0.000	+0.013	0.000	0.002	+0.015	0.003
			d_{xz}	0.001	0.007	+0.038	0.000	0.005	+0.045	0.003	0.002	+0.051
			d_{yz}	-0.011	+0.030	0.008	-0.013	+0.036	0.006	-0.015	+0.047	0.004

Continued in next page...

Continued from previous page...

Kind	\mathbf{r}_{ij} (in Cartesian coord.)	Sublattice	$U_{\text{eff}} = 0.0 \text{ eV}$			$U_{\text{eff}} = 1.5 \text{ eV}$			$U_{\text{eff}} = 3.0 \text{ eV}$			
			d_{xy}	d_{xz}	d_{yz}	d_{xy}	d_{xz}	d_{yz}	d_{xy}	d_{xz}	d_{yz}	
$t_{\text{NNN}}^{\text{IV}}$	$(+d, -2d, +d)$	1 \rightarrow 4	d_{xy}	+0.012	0.007	-0.030	0.009	0.008	-0.035	0.005	0.008	-0.041
			d_{xz}	0.007	0.008	0.006	0.008	0.009	0.008	0.008	+0.011	0.008
			d_{yz}	-0.030	0.007	0.003	-0.035	0.008	0.007	-0.041	0.008	-0.012
$t_{\text{3NN}}^{\text{I}}$	$(0, +2d, -2d)$	1 \rightarrow 2	d_{xy}	0.007	-0.013	-0.014	0.007	-0.014	-0.015	0.008	-0.015	-0.017
			d_{xz}	0.008	0.006	0.006	0.009	0.008	0.007	-0.011	+0.011	0.009
			d_{yz}	-0.014	-0.016	-0.034	-0.015	-0.018	-0.030	-0.017	-0.020	-0.022
$t_{\text{3NN}}^{\text{II}}$	$(-d, +d, 0)$	1 \rightarrow 1	d_{xy}	-0.045	0.006	-0.012	-0.046	0.007	-0.013	-0.046	-0.010	-0.013
			d_{xz}	+0.012	0.008	0.001	+0.013	0.009	0.001	+0.013	+0.012	0.002
			d_{yz}	0.006	-0.015	0.008	0.008	-0.017	0.009	+0.010	-0.018	+0.012